Characterization of DBD Plasma Actuators Performance without External Flow – Part I: Thrust-Voltage Quadratic Relationship in Logarithmic Space for Sinusoidal Excitation

David E. Ashpis*
National Aeronautics and Space Administration, Glenn Research Center, Cleveland, Ohio, 44135

and

Matthew C. Laun†
HX5 Sierra LLC, Glenn Research Center, Cleveland, OH, 44135

We present results of thrust measurements of Dielectric Barrier Discharge (DBD) plasma actuators. We have used a test setup, measurement, and data processing methodology that we developed in prior work. The tests were conducted with High Density Polyethylene (HDPE) actuators of three thicknesses. The applied voltage driving the actuators was a pure sinusoidal waveform. The test setup was suspended actuators with a partial liquid interface. The tests were conducted at low ambient humidity. The thrust was measured with an analytical balance and the results were corrected for anti-thrust to isolate the plasma generated thrust. Applying this approach resulted in smooth and repeatable data. It also enabled curve fitting that yielded quadratic relations between the plasma thrust and voltage in log-log space at constant frequencies. The results contrast power law relationships developed in literature that appear to be a rough approximation over a limited voltage range.

Nomenclature

f	frequency
k	anti-thrust coefficient
V	voltage
T	thrust

Actuator geometry parameters - see Appendix A

Acronyms:

AC	Alternating Current
DC	Direct Current
RH	Relative Humidity
DP	Dew Point
kV	kilovolts

Subscripts:

p-p	peak to peak

I. Introduction

A DIELECTRIC Barrier Discharge (DBD) actuator is an aerodynamic active flow control device that consists of a pair of electrodes separated by a dielectric. One electrode is exposed to the flow and the other is covered. Alternating Current (AC) voltage in the kilovolt (kV) range is applied to the electrodes and creates weakly ionized surface discharge plasma on the exposed electrode edge towards the buried electrode direction (Fig. 1). There are usually two modes of operation. Conventional DBD operation involves application of an Alternating Current (AC)

* Research Aerospace Engineer, Propulsion Division, 21000 Brookpark Road. AIAA Associate Fellow.
† Electrical Engineer, Facilities Division, 21000 Brookpark Road, Non-member.

voltage waveform in the kilohertz frequency range, with or without modulation or pulsing. In this mode, referred to as "AC-DBD", heat generation is usually insignificant and the actuator generates momentum in the form of a wall-jet parallel to the surface. The wall-jet momentum coupling with the external flow is the foundation for active flow control. The other mode of DBD operation involves applying voltage consisting of ultra-short, repetitive pulses. The pulses are usually several nanoseconds wide and the repetition rate ranges from a few hundred hertz to a few hundred kilohertz. In this mode of operation, generally referred to as "NS-DBD," when the pulses are symmetric the generated momentum is negligible but there is a fast, localized heating of the gas that creates pressure waves or even shock waves. The repetition generates pressure oscillations that are used for active flow control. When the pulses are asymmetric, NS-DBD can generate wall-jet momentum. For the AC-DBD actuators, see review articles by Moreau[1], Corke et al[2,3,4], Benard and Moreau[5], and Kotsonis[6]. For the NS-DBD actuators, see the paper by Roupassov et al [7]. Combinations of AC-DBD and NS-DBD were also reported by Starikovskiy et al[8].

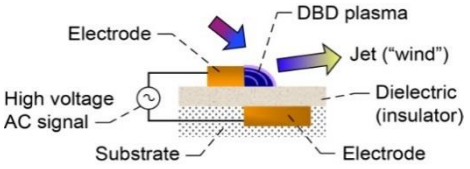

Figure 1. Schematic of a DBD Plasma Actuator

The interest is to characterize the aerodynamic and electrical performance of the actuator. Generally, it is performed without external flow. Measurements of the plasma-generated jet as function of electrical supply voltage and current for specified waveforms, frequency, modulation and pulsing are performed for specific actuator geometries and dielectric materials.

This paper is focused on the thrust measurements of AC-DBD actuator. The approach builds on our prior work on thrust measurements, Ashpis and Laun [9,10,11] (Ref. 11 is slightly revised version of Ref. 10).

II. The Thrust of the DBD Actuator

The thrust of the DBD plasma actuator is a good metric for its aerodynamic performance. The reason is that in active flow control applications the main interest is in the momentum injected into the flow by the actuator. Pneumatic actuators use a momentum coefficient as performance and characterization parameter (e.g., Glezer and Amitay[12]).

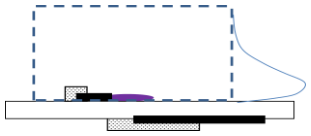

Figure 2. Control volume for thrust evaluation

The momentum can be calculated from integration of measured flow velocity profiles, or from direct thrust measurement. From a control volume consideration shown in Figure 2, the thrust is approximately equal to the net momentum generated by the actuator[13,14]. The difference is the shear force on the surface. There is also a component of the force in the surface-normal direction which is not considered here. There are some issues and difficulties associated with direct velocity measurements[10], usually performed with Pitot tube, PIV (Particle Image Velocimetry) or LDV (Laser Doppler Velocimetry). It makes thrust measurement attractive because of its simplicity. The thrust can be measured by a balance or a load cell. Because load cells with the required resolution, range and tare weight capacity are hard to find or non-existent, an analytical balance is useful for this suppose. For example, when an actuator is placed on the balance with the jet facing up as shown in Figure 3, the balance reading is the sum of the forces generated by the plasma and the shear forces on the surface. If the shear forces are sufficiently small to be neglected, then the thrust will be close to the momentum[13].

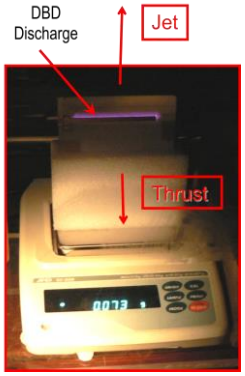

Figure 3. Setup of an actuator on an analytic balance

Although much simpler than velocity measurements, there are many issues and difficulties associated with thrust measurements. We have recently developed an approach for achieving reliable and repeatable results. The issues and the new approach are discussed in a comprehensive manner in Ashpis and Laun[10,11]. As a brief summary, the issues that our approach addressed were non-repeatability, fluctuations, and drift in time, dependence on actuator conditioning profile ("burn-in"), the manner of applying the voltage, dynamic forces caused by charged lead wires, effect of the surrounding enclosure, and isolation of the plasma generated momentum from other effects. Our approach includes (a) a new type of test setup where the actuator is suspended in the room, (b) a burn-in procedure, (c) a data acquisition procedure, and, (d) correction of the measured data using a proposed anti-thrust hypothesis. These approaches were employed in the current work.

Although it is known that discharges, and hence the thrust, strongly depend on humidity, it was a neglected area in literature, where the value of the humidity in reported tests results was rarely

noted. A comprehensive study on effect of humidity on the wall-jet velocity was performed by Benard et al [15]. They performed experiments with relative humidity ranging from 40 to 98 percent, and showed that the wall-jet peak velocity decreases with increased humidity. We have observed[10] a similar trend, and showed that humidity can increase thrust by as much as 41% between relative humidity of 50% (dew point 57 °F) and 18% (dew point 33 °F). Effects of humidity were also studied by Wilkinson et al[16]. They found that the trend was dependent on the dielectric material type as well as on water absorption in the dielectric.

Note that it is not clear what the relevant humidity parameter should be. For effect of humidly in the air, it may not be the relative humidity. The dew point temperature is a more appropriate parameter as it is related to the volume fraction of water in the air. An additional parameter may be needed to accurately characterize effects of water absorption in the dielectric. Evaluation of the appropriate humidity characterization parameter for DBD discharges is left for separate work.

The testing reported herein were performed at low ambient humidity. In this report we show results with dew point in the range 37 to 39 °F (corresponding relative humidity was 26 to 22 %). The low humidity ensured repeatable results and uniform discharges with minimal fillaments[10].

III. Test Setup

The test setup is identical to the one used in Ashpis and Laun[10], and its description is repeated here and shown in Figure 4. An image of the laboratory setup is shown in Figure 5. We have developed this setup to counter some of the problems associated with our testing in an enclosure. The AND® analytic balance we used (A&D Company, Limited, Japan, Model AND GX-1000) has linear accuracy of ±3 mg and repeatability of 1 mg. It is equipped with an under-hook that enables it to measure hanging loads. The balance was installed on a small aluminum platform attached to the laboratory ceiling. The balance was thermally insulated with an enclosure made from polystyrene foam sheets to minimize thermal drift. The air temperature in the enclosure was monitored with a thermocouple. The actuator test article was suspended with thin nylon monofilaments (fishing line) attached to a metal frame that was hung on the balance's hook.

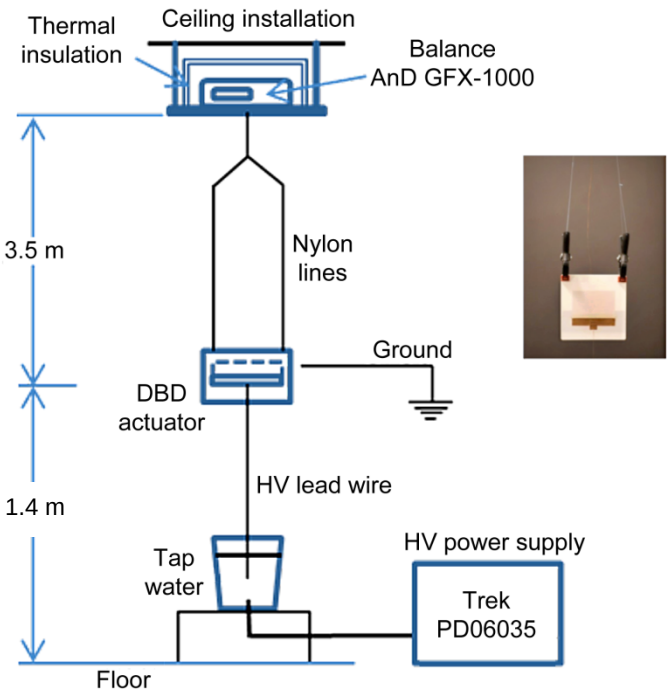

Figure 4. Suspended DBD actuator test setup schematic (not to scale).

The test article was installed as far as practical from nearby objects. The floor underneath the test article consisted of grounded metal plates. The surrounding objects included metal cabinets, workbenches, metal and acrylic structures, and cement walls and floors with embedded steel reinforcing. The balance was installed about 3.5 m above the actuator,

and testing revealed there was no detectable EMI interference by the balance due to the actuator. The nearest distance to adjacent objects was 1.2 m. Typically, the distances were in the range of 1.5 to 2.0 m. The actuator was suspended about 1.4 m above the floor. After gaining some experience, we were able to minimize movements of the suspended test article that would affect the balance reading.

We used a Trek Inc. high voltage amplifier Model PD06035. Its maximum slew rate is 725 V/μs (at no load, 10 to 90 percent typical) and the DC gain is 3000 V/V. The effective slew rate was reduced to 220-260 V/μs after the electrical actuator load was applied. The range of its working frequencies starts at DC. The combination of its frequency and voltage output range is limited by the effective slew rate. The sinusoidal input waveform was supplied with a synthesized signal generator, Stanford Research Systems (SRS) Model DS345m. The Trek is equipped with a visible indicator to warn of output waveform distortion. We also simultaneously used an oscilloscope to detect output voltage waveform distortion.

We used the factory-supplied output cable, Trek part number 43466B, with a total length of approximately 2 m. A section of the cable, approximately 1.5 m long, was routed through 1 in I.D. acrylic tube raised about 4 in above the metal floor with antistatic Polyethylene foam risers for extra insulation. This arrangement was kept constant at the various tests so as not to vary the capacitance between the cable and the surroundings.

The high voltage was fed to the powered actuator electrode through a force-decoupling, conductive-liquid, interface arrangement, as follows. The high voltage 28 AWG copper feedwire lead was suspended vertically with a metal counterweight into a styrene cup containing tap water that submerged the counterweight completely below the surface. The high voltage was fed from the output cable of the power supply into the water via a stainless steel needle that pierced the bottom of cup. Sufficiently ionized tap water was selected due to its conductivity, and allowed charging of the actuator electrode with minimal impedance. Dynamic forces caused by the lead wire charging, were minimized below detectable levels. The ground 28 AWG copper feedwire lead was connected to the covered electrode via a thinner 40 AWG copper wire suspended in an approximate catenary shape to minimize forces.

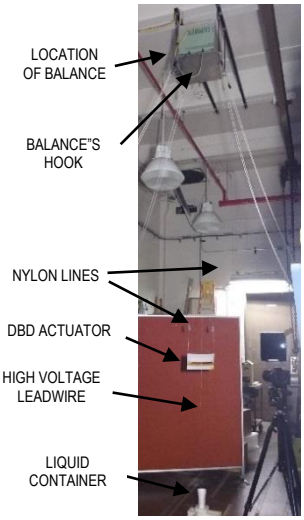

Figure 5. View of the suspended DBD actuator test setup

The high voltage was measured with the Trek's built-in voltage monitor (3000:1 ratio). It is based on a high performance voltage divider. It adequately represents the AC voltage on the electrodes within the moderate frequency ranges used.

We used a Nikon digital camera Model D300S to take still images of the discharges. Camera setting of the images shown herein were F4.5, ISO 200, and exposures of 5 s or 30 s, as noted. Darkened room was required.

The balance readings were recorded using a LabVIEW (National Instruments) application. The balance provides continuously-averaged load measurements 10 times per second. Testing performed on the balance revealed that this averaging occurs for time-varying loads at frequencies above 2 Hz. Alternatively, time-accurate readings can be acquired for loads that vary below 0.5 Hz. The accuracy of the AND® balance is accomplished via a servo loop activating an electromagnetic coil that maintains the deflection of the internal beam at zero. The electrical current to the coil is nearly linear with the load. This construction has a particular advantage relevant to our tests, as the static forces of the lead wires are null, because there is no steady state deflection that will cause stress forces in the lead wires.

The actuators we used in the study reported here were made of High-Density Polyethylene (HDPE) dielectric. The dielectric properties (see Appendix A) are close to those of PTFE, Dielectric Constant $\varepsilon = 2.3$, making it a low capacitance class of actuators that were shown by others to allow application of high voltage to achieve high levels of thrust. We found that this material does not exhibit sudden pin-hole type burn-through that we encountered while using PTFE, PEEK, and other polymers. The HDPE exhibited excellent durability over long periods of time.

The tests reported here are made with three actuator test articles that differed mainly with the thickness of the dielectric, nominal 1/16, 1/8, and 1/4 inch. There were minimal variations in the electrodes offset gap dimensions, as they are difficult to control when constructed by hand. The HDPE dielectric material used were roughly 6 in x 12 in plates, and the active length of the electrode was approximately 10 in, largely determined by the spanwise length of the covered electrode. Precise dimensions and other construction details of the actuators used are listed in Appendix A.

An important feature of the construction was insulating the end edges of the exposed electrode. The insulation of the edges is critical to inhibit plasma formation on the electrode end corners. This promotes only measuring the thrust due to plasma formation on the linear edge of the exposed electrode. We have developed a technique using repetitive

application of several (typically 3 to 4) thin layers of Corona Dope[‡], letting each layer dry between applications, and stacking the layers in a stepped manner. Other methods of insulating the electrode edges, for example using insulating tape or putty, proved ineffective. In addition, the upstream side of the exposed electrode was insulated with Kapton® tape to prevent discharges.

The ambient humidity, temperature, and pressure were measured with a combination probe and a recorder, Omega (Newport) Model No. iServer Micorserver iBTHX-W-5.

In our testing, there was no attempt made to control the ambient humidity. It was set by the weather and the conditions in the building. The HVAC system controlled the room temperature but not the humidity. Our test spanned a period of about four months where the atmospheric humidity changed. The humidity was nearly constant over the various test time intervals. We have recorded the temperature, relative humidity, and the dew point. The test were performed when atmospheric humidity was relatively low.

IV. Thrust Measurement Methodology

We have used the methodology developed in prior work reported in Ashpis and Laun[10] and described there in detail. We use pure sinusoidal wave form and have followed the measurement procedure summarized as follows.

A. Burn-in and voltage-frequency sweeps

We first perform a burn-in by gradually exposing the actuator to the maximum voltage and the maximum frequency in the range. We have swept from high to low frequency, and stepped down from high to low voltage. The thrust data is continuously recorded at approximately 10 Hz determined by the balance hardware. Dwell time at each frequency-voltage point was 60 sec. That thrust is calculated by averaging the data within each 60 sec step. Using a window smoothing function.

\

B. Waveform distortion monitoring

The distortion of the sinusoidal waveform was monitored mainly via the indicator light on the Trek power supply. It was compared to oscilloscope waveform display, which verified the onset of slew-rate distortion. The data was retained only for non-distorted waveforms.

The range of voltages and frequencies yielding non-distorted waveforms used was constrained by the performance specifications of the power supply, mainly governed by its slew rate, the actuator and feed line load impedance, and the breakdown voltage of the actuator dielectric.

C. Anti-Thrust Correction

The raw data results were adjusted by the anti-thrust hypothesis correction method[10].

$$\text{Total Thrust} = \text{Plasma Thrust} + \text{Anti Thrust} \tag{1}$$

The total thrust is the thrust as measured by the balance. The plasma thrust is the thrust associated with the discharge on the exposed electrode that generates the momentum. The second term on the right hand side was termed “anti-thrust” because it is always negative and is represented by the parabolic curve fit,

$$\text{Anti Thrust} = kV^2 \tag{2}$$

We performed the anti-thrust corrections by performing an initial frequency and voltage sweep in the stepped manner[10]. Parabolic curve fitting of data acquired at frequencies ranged from 4 to 64 Hz, depending on each case. The appearance of unwanted plasma discharges was determined by examining photographs taken at each voltage step, with the objective to maximize the AC frequency used for the anti-thrust correction, to minimize drift and increase accuracy[10]. We also need to stay above 2 Hz, which is the low limit of the balance averaging range; below that value the balance provides time series data.

[‡] Super Corona Dope®, MG Chemicals Inc. Cat. No. 4226-1L

V. Results

A. Experimental data results corrected for anti-thrust

The results of measurements are shown in figures 6 to 8 for the three actuator thicknesses (nominal 1/16. 1/8, and 1/4 inch, respectively). The figures show the plasma thrust as function of voltage for fixed frequencies. The symbols show the experimentally-acquired data corrected to anti-thrust according to Eqs. (1) and (2). The data is plotted on log –log scales. The conversion of thrust (grams) to normalized thrust (mN/m) is indicated on the figures, it is assumed that the active length of the discharge is equal to the spanwise length of the covered electrode (see discussion in Appendix A).

Some of the tests were repeated on different dates for the same parameters. Figures 7 (1/8 in. actuator) shows excellent agreement of data repeated at 2 kHz.

Figure 8 (1/4 in. actuator) includes several repetitions of data acquired on different dates. The repetition of the 3 kHz data is excellent. The repetition of the 2 and 1 kHz cases is excellent except for slight deviation of the two lowest voltage points. The repetition of the 0.5 kHz cases is very good to excellent

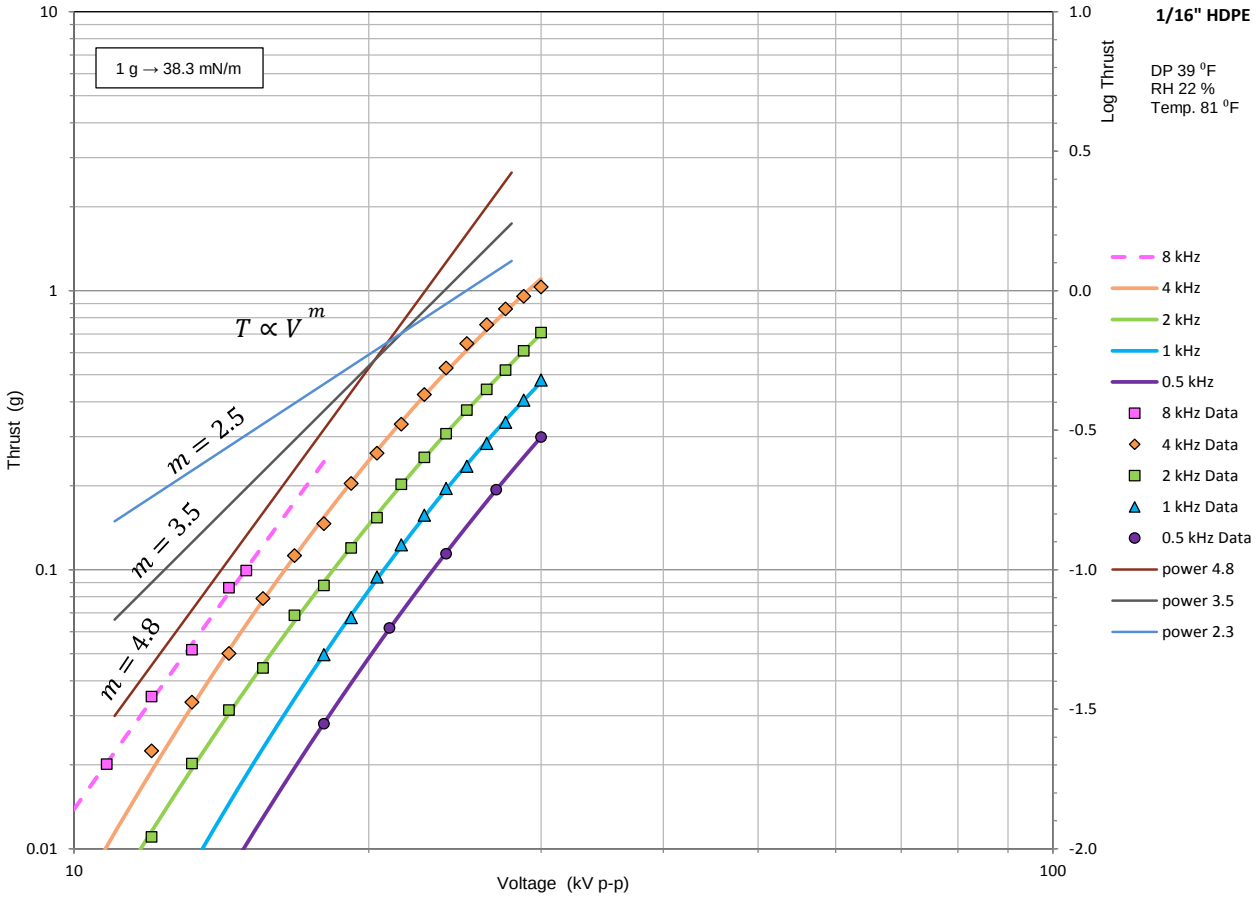

.

Figure 6. Plasma thrust of the 1/16" thick actuator as function of voltage for fixed frequencies on log-log scale. Pure sine wave applied voltage. Symbols show experimental data corrected to anti-thrust. Solid curves are quadratic curve fits. Power-law lines are shown for reference

Table 1. Humidity values for the test cases

Actuator Nominal thickness	Dew Point (DP)	Relative Humidity (RH)	Temp
inch	° F	%	° F
1/16	39	22	81
1/8	37	26	74
1/4	37	26	74

The values of the room humidity corresponding to the three data sets are shown in Table 1. Although not all the tests were performed at the same time, there were very small humidity variations.

B. Quadratic curve fits

Curve fits performed in the log-log plane result in excellent fit to quadratic curves. Microsoft Excel® polynomial "Trendline" feature was used.

The quadratic representations at constant frequency are

$$\log(T) = a\,[log(V)]^2 + b[\log(V)] + c \tag{3}$$

The coefficients of the quadratic relationship a, b, and c for the various cases are listed in Table 2.

The R-Squared values, as calculated by Microsoft Excel®, were quite close to 1 showing high degree of fit. The lowest value of R-Squared was 0.9997, while the highest was 0.9999.

As can be seen visually, the curves are smooth and orderly, they are nested within each other and do not overlap. The superior curve fit is enabled by the anti-thrust correction. Without the anti-thrust correction, it was not possible to curve-fit with a similar degree of fit. Similarly, when thrust data from slightly distorted voltage waveform was included, a rapid deviation from the quadratic curves occurred.

Table 2.
Quadratic curve fit coefficients.
$\boldsymbol{\log(T) = a\,[log(V)]^2 + b[\log(V)] + c}$

Actuator	f (kHz)	a	b	c
1/16"	0.5	-2.820	12.328	-12.583
	1	-3.483	13.919	-13.287
	2	-2.688	11.352	-11.059
	4	-3.300	12.869	-11.767
	8	-0.236	5.410	-7.031
1/8"	0.25	-3.158	13.977	-14.759
	0.5	-3.307	14.217	-14.546
	1	-3.766	15.211	-14.780
	2	-3.349	13.636	-13.182
	3	-3.358	13.628	-13.141
	4	-3.281	13.324	-12.769
1/4"	1	-8.785	32.672	-30.248
	2	-6.282	23.973	-22.520
	3	-6.054	23.035	-21.509
	4	-4.626	18.321	-17.553
	8	-7.313	26.571	-23.800

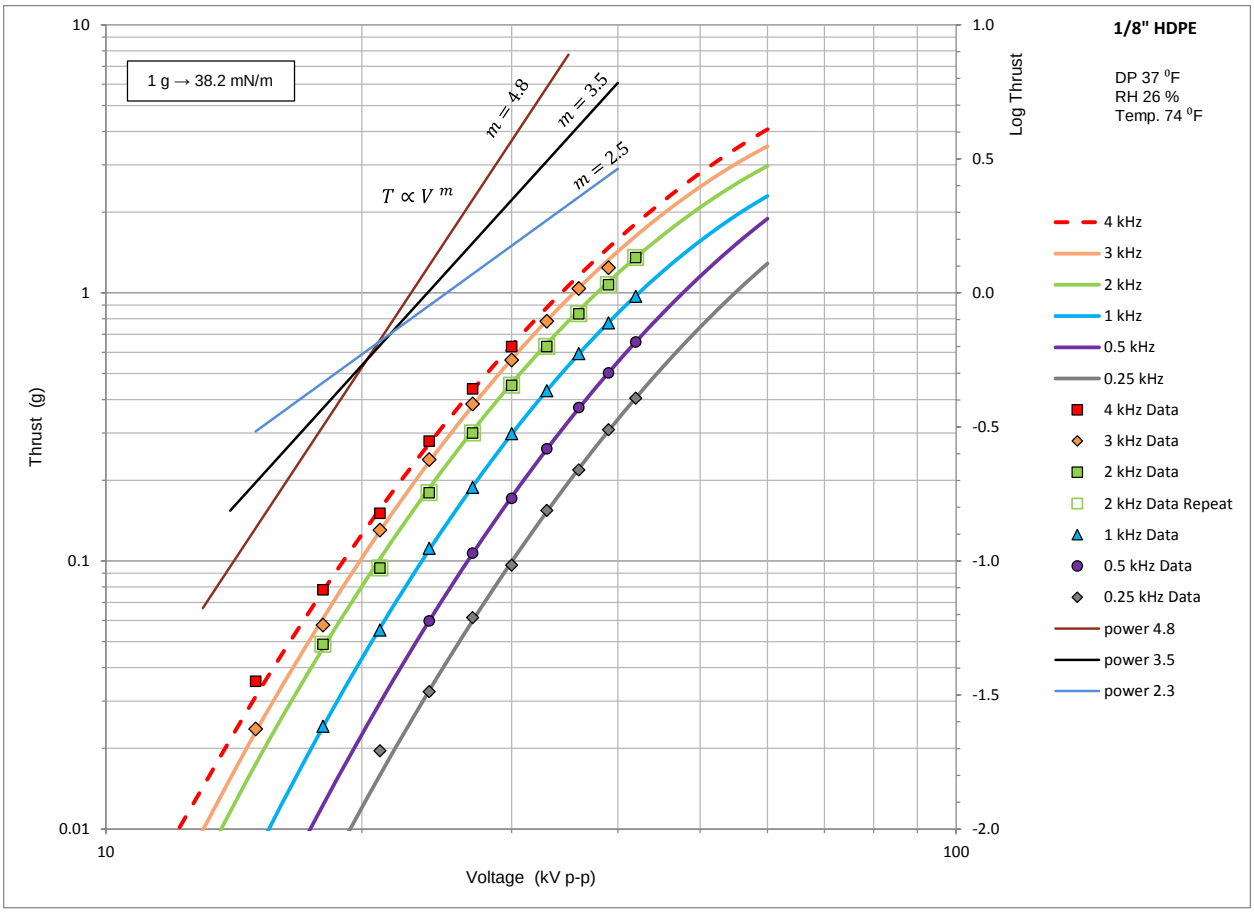

Figure 7. Plasma thrust of the 1/8" thick actuator as function of voltage for fixed frequencies on log-log scale. Pure sine wave applied voltage. Symbols show experimental data corrected to anti-thrust. Solid curves are quadratic curve fits. Power-law lines are shown for reference.

VI. Discharge imaging

We have imaged discharges with a camera for the 1/8 in actuator. The imaging was performed at a later date, and there was some deterioration in the right hand corner edge. The images are shown in Figures 9 to 12.

Figure 9 displays images of discharges for (a) a range of voltages at a fixed frequency of 2 kHz, and (b) for several frequencies at constant voltage of 27 kVp-p. The corresponding curves can be identified in Figure 7. Each series of images in Figure 9 are at a fixed exposure regardless of the discharge intensity for. All the constant frequency images were taken with a camera setting of 5 s exposure, ISO 200 and F4.5. All the constant voltage images were taken with a camera setting of 30 s exposure, ISO 200 and F4.5. The reader of the electronic version can enlarge the figure and examine the discharge details. Inevitable minor non-uniformity and minor mini-filament are observed, they are caused by unavoidable imperfections in the edge of the copper tape electrodes, which are hand cut. The filaments are very small and do not affect the general excellent uniformity of the discharge. There are none, or a minimal number, of larger filaments.

Note that the straight edge of the electrode may appear curved due to slight spanwise cylindrical curvature of the actuator and the viewing angle

Figure 10 displays composite strips made of sections of the images side by side for constant frequency of 2 kHz. It makes it easy to follow the progression of the discharge with voltage. One composite strip is with the fixed exposure,

and the other was digitally processed and its Gamma value was changed, to enhance the visibility of the low intensity discharges. Figure 11 similarly shows composite strips of the discharge at constant voltage of 27 kVp-p.

Figure 12 is a similar composite strip showing images at constant thrust of 300 mg. The pairs of frequency and voltage values resulting in the constant thrust are shown. Figure 12 camera settings were 30 s exposure time, ISO 200 and F4.5.

Note that the spanwise location of each image in a composite strip is at its original location. The edge image sections may also reveal end edge discharges, which can also occur to a lesser extent above the insulating layers of corona dope.

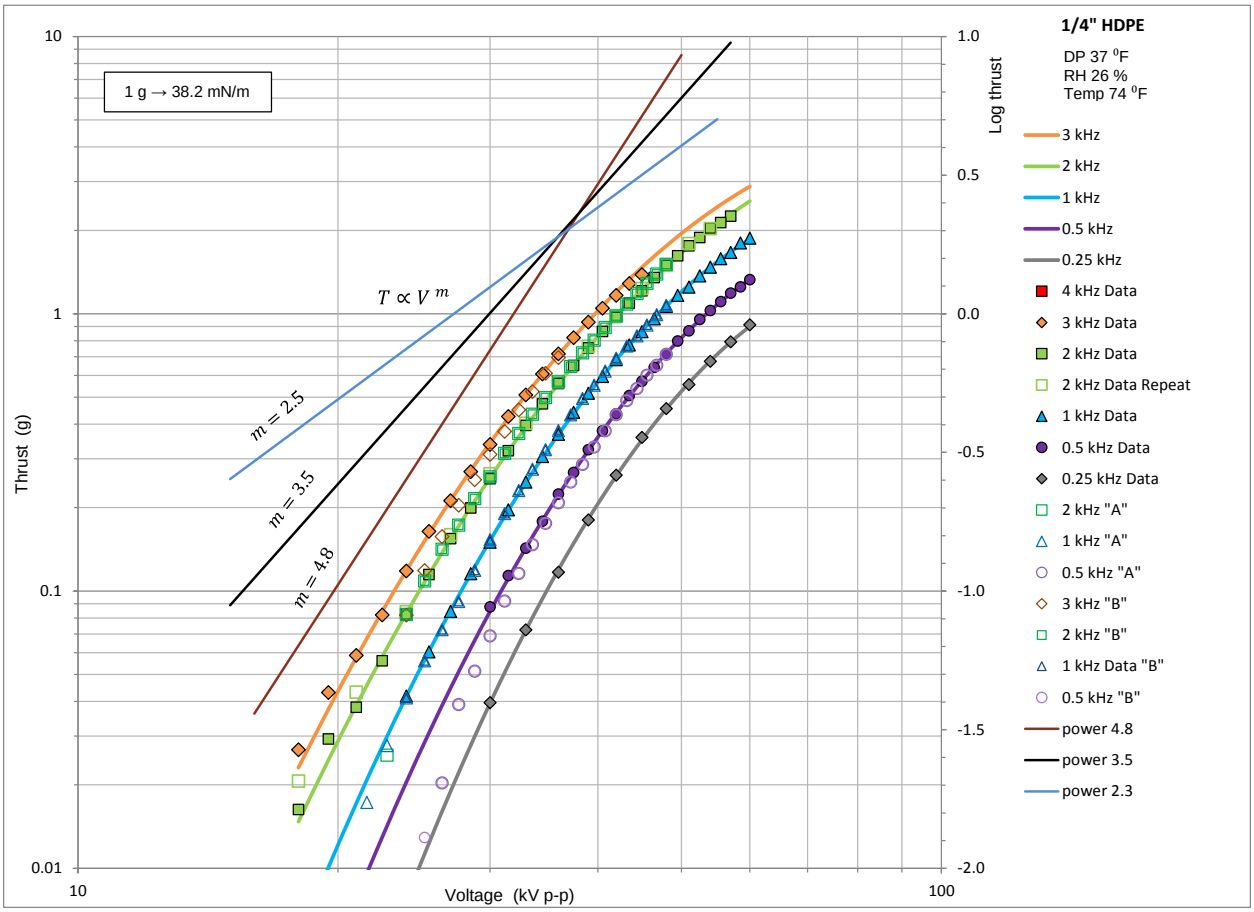

Figure 8. Plasma thrust of the 1/4" thick actuator as function of voltage for fixed frequencies on log-log scale. Pure sine wave applied voltage. Symbols show experimental data corrected to anti-thrust. Solid curves are quadratic curve fits. Power-law lines are shown for reference.

VII. Summary and Conclusion

Simultaneously using a careful experimental approach, specific actuator fabrication methods, pure sinusoidal excitation, and anti-thrust hypothesis correction, yields excellent quadratic curve fits in the $log\,(Thrust) - log\,(Voltage)$ plane for constant frequencies.

Our results contradict the commonly accepted curve fit in literature which is a power law, $T \propto V^{m}$, at constant frequency.

Several values for *m* can be found in literature for sinusoidal voltage input. Thomas et al[17] proposed $m = 3.5$ for low voltage range, and $m = 2.3$ for higher voltage range. Wilkinson et al[16] found that $m = 4.8$ fits some of their data (dielectric material dependent). Zito et al[18] observed *m = 2*.2, 3.4, 3.6, and 6.6 for microscale DBD actuators.

Our results show that none of these values is sole representative of the thrust-voltage relationship over the full voltage range, and that the relationship is actually quadratic in the log-log plane. It was shown by Wilkinson et al[16], by adapting electrostatic field analytical solutions, that the electric field contributes a logarithmic relationship to capacitance of an actuator-like capacitor. It helps explain the appearance of a logarithmic term in the thrust data.

The deviation from a quadratic curve observed by others can be explained by the following reasons:

(a) Non sinusoidal waveforms, sinusoid distortion, and harmonics. In particular, use of power supplies that employ transformers can degrade the signal quality by adding harmonics.
(b) Construction of DBD actuators that makes them prone to filamentary discharges.
(c) Operation in moderate-to-high humidity environment that makes the discharges non-uniform, patchy, filamentary, time-unstable, and non-repeatable[10].
(d) Edge effects that contaminate the straightedge plasma contribution to thrust.
(e) No compensation for anti-thrust from non-visible electric forces.
(f) No separation of desired edge-generated plasma thrust from parasitic plasma thrust sources, and other sources of proximal and electrostatic interaction that affect the balance's thrust reading.

Obtaining a quadratic thrust-voltage relationship in log-log space with sinusoidal excitation of DBD actuators in a dry environment can be now considered a measure of quality of the actuator construction, the measurement system, and proper isolation of the plasma thrust generated by the electrode spanwise edge.

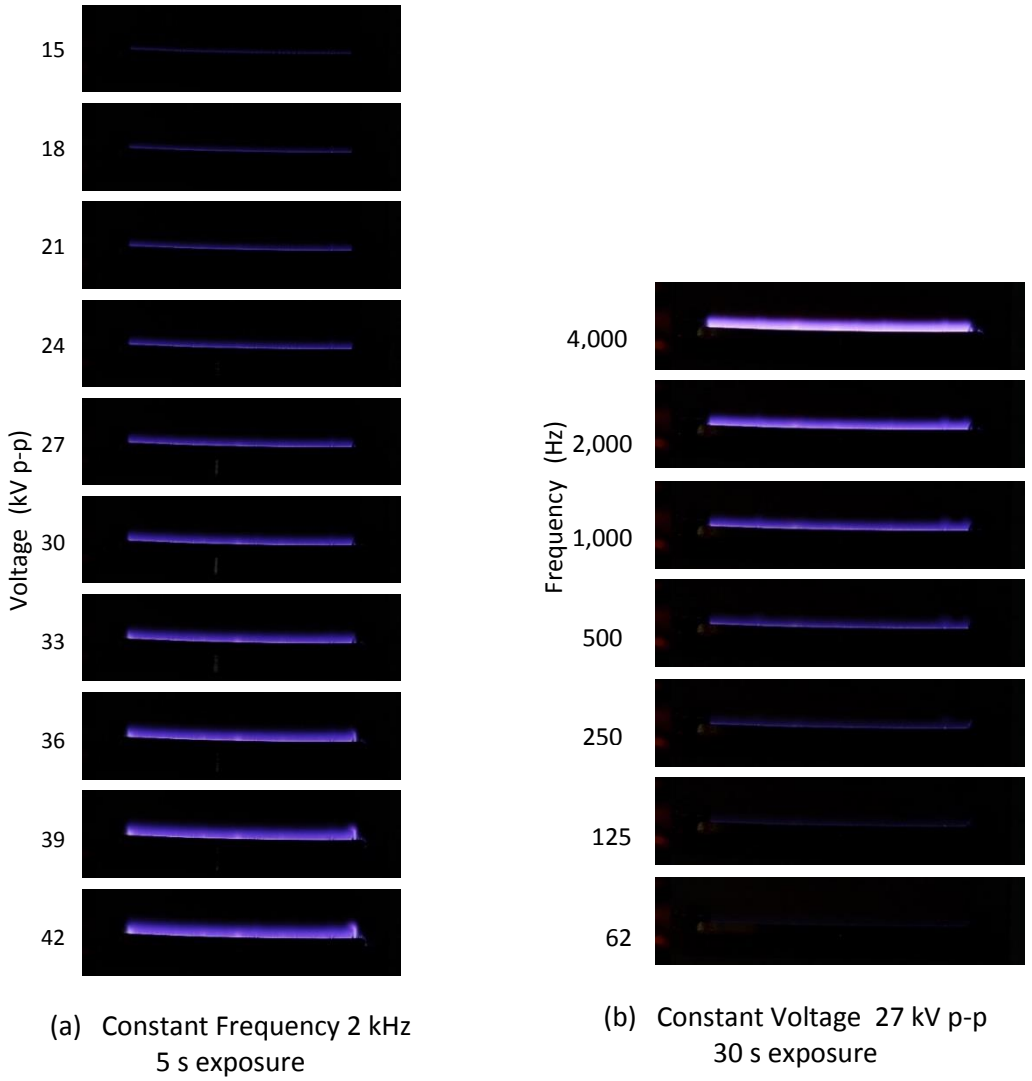

Figure 9. Images of the discharge for the 1/8" thick actuator. Pure sine wave applied voltage. (a) Constant frequency of 2 KHz. Camera settings: 5 s exposure, ISO 200, F4.5 (b) Constant voltage of 27 kV p-p. Camera settings: 5 s exposure, ISO 200, F4.5. The viewing angle and slight spanwise cylindrical curvature of the actuator makes the straight electrode edge appear curved.

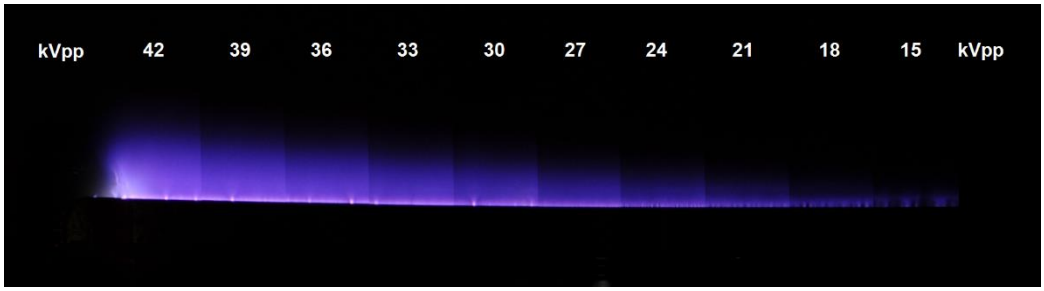

(a) Fixed exposure. f = 2 kHz

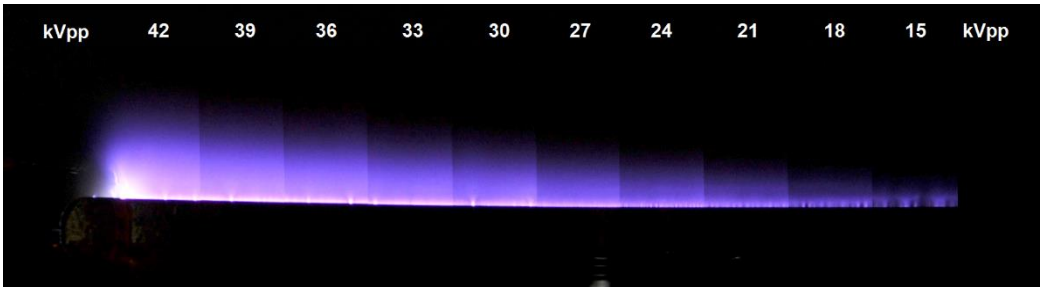

(b) Gamma enhanced. f = 2 kHz

Figure 10. Composite images of the discharge for the 1/8" thick actuator. Pure sine wave applied voltage. The images consist of sections of the various individual images with and without Gamma enhancement. Constant frequency 2 kHz. (a) Fixed exposure (5 s, ISO 200, F4.5) (b) With Gamma enhancement

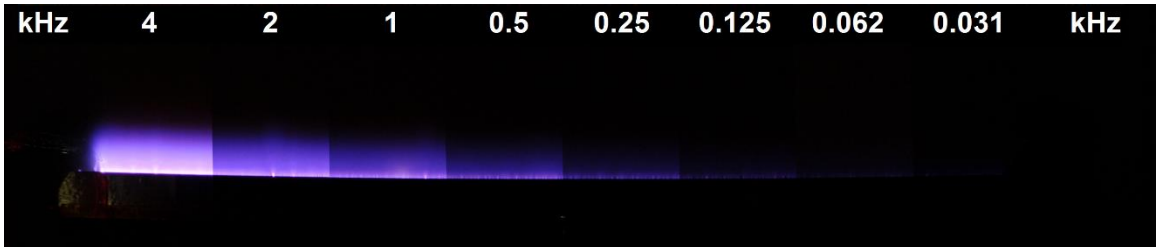

(a) Fixed exposure. V = 27 kV p-p

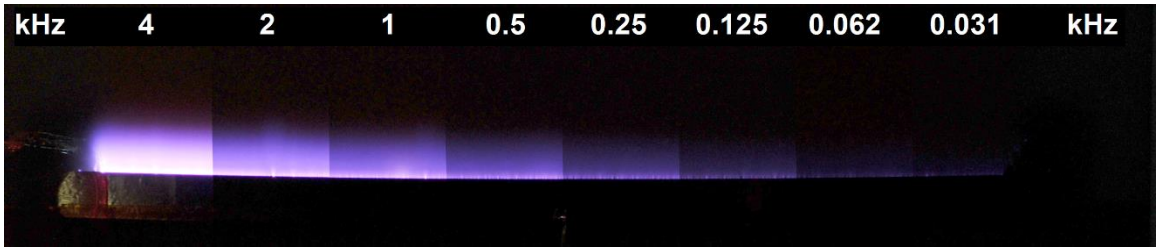

(b) Gamma enhanced. V = 27 kV p-p

Figure 11. Composite mages of the discharge for the 1/8" thick actuator. Pure sine wave applied voltage. The images consist of sections of the various individual images with and without Gamma enhancement. Constant voltage 27 kVp-p. (a) Fixed exposure (30 s, ISO 200, F4.5) (b) With Gamma enhancement

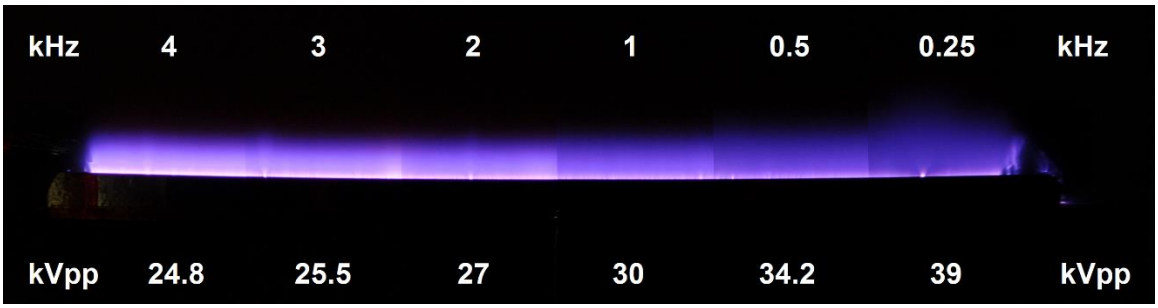

(a) Fixed exposure. T = 300 mg

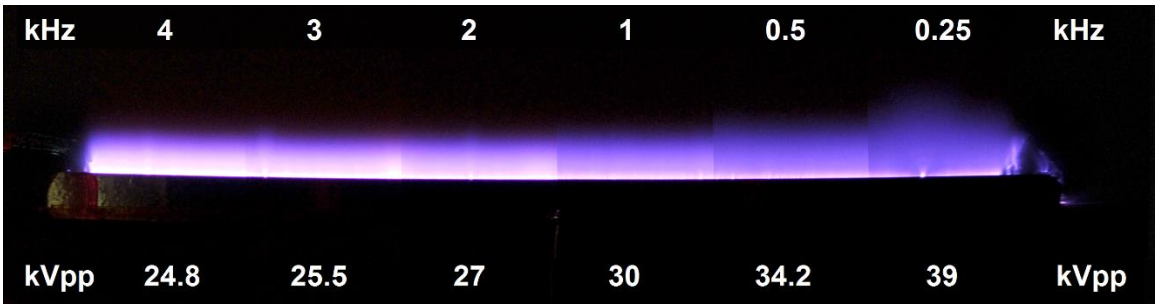

(b) Gamma enhanced. T = 300 mg

Figure 12. Composite images of the discharge for the 1/8" thick actuator. Pure sine wave applied voltage. The images consist of sections of the various individual images with and without Gamma enhancement. Constant thrust. *T*= 300 mg. (a) Fixed exposure (30 s, ISO 200, F4.5) (b) With Gamma enhancement

Appendix A—Actuator Dimensions and Properties Information

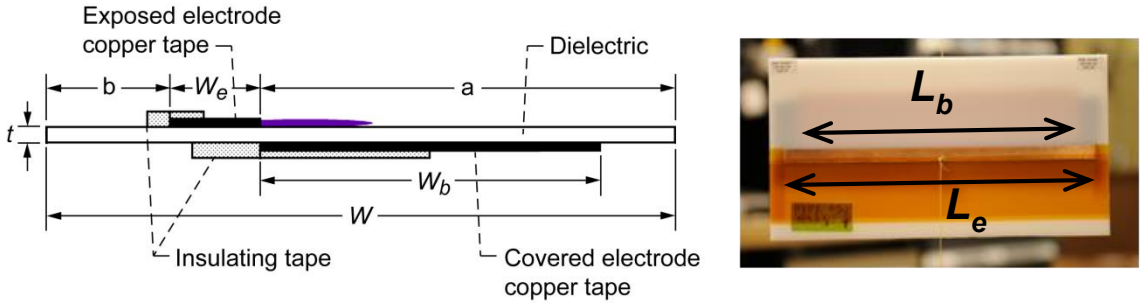

Figure 21.—DBD plasma actuator test article—geometry and dimensions.

TABLE A1.—ACTUATORS DIMENSIONS AND INFORMATION[§]

Designation	*t* *(Nominal)*	*t*	W_e	W_b	L_e	*W*	*a*	*b*
	inch	mm	mm	mm	mm	mm	mm	mm
HDPE #5	1/16	1.53	12.7	51	282	154	86.5	54.0
HDPE #7	1/8	3.16	12.0 12.8	48	283	164	81.0	59.0
HDPE #3	1/4	6.09	12.0	48	254	154	76.5	64.5

Designation	*t* *(Nominal)*	L_e (exposed electrode)	L_b (covered electrode)	$L_{e\text{-uninsulated}}$ (exposed electrode)	Thrust *T* to T/L_e conversion factor	Thrust *T* to T/L_b conversion factor	Thrust *T* to $T/L_{e\text{-uninsulated}}$ conversion factor
	inch	mm	mm	mm	g to mN/m	g to mN/m	g to mN/m
HDPE #5	1/16	282	256	218	34.78	38.31	44.98
HDPE #7	1/8	283	257	249	34.65	38.16	39.38
HDPE #3	1/4	254	256.5	259	38.61	38.23	37.86

Actuator geometries and materials are as shown in Figure 21.

Table A1 lists dimensions of the actuator components.

Table A1 also lists calculated conversion (multiplication) factor to convert from thrust in grams (g) to normalized thrust (thrust per unit length) in millinewton per meter (mN/m).

L_e is the spanwise length of the exposed electrode, L_b is the spanwise length of the covered electrode. The actuators were constructed such that L_e is longer than L_b. $L_{e\text{-uninsulated}}$ is uninsulated length of the exposed electrode not covered by the corona dope.

Several choices can be made for determination of the active length of the plasma for purpose of normalizing the thrust with the active spanwise length of the plasma. The plasma is largely limited by the spanwise extent of the covered electrode, but the electric field at the ends still allows some discharge, corona, and ion wind, that can generate thrust. Therefore other normalizing lengths potentially can be used. The table shows the respective conversion factor from thrust in gram to mN per meter for each actuator based on the three lengths. The value based on the covered electrode length are the ones indicated on Figures 6 to 8.

[§] Due do fabrication inaccuracies the sum $a+b+W_e$ might not equal *W*.

The dielectric material, electrode material, and electrode insulation material used are also listed below.

a) Dielectric material:
High Density Polyethylene (HDPE). Table A2 lists the vendor's part numbers.

TABLE A2: McMaster-Carr HDPE part numbers.

Designation	*t* *(Nominal)*	*P/N*
	inch	
HDPE #5	1/16	8619K995/8619K747
HDPE #7	1/8	8619K996/8619K748
HDPE #3	1/4	8619K461/8619K751

HDPE Electrical properties:[**]
Dielectric Constant: 2.3 at 1 kHz
Dielectric Strength: 22 MV/m
Dissipation Factor: 0.0005 at 1 kHz

b) Electrode material:
Copper tape with conductive adhesive. 3M No. 1181
Copper thickness: 0.04 mm (1.4 mil)
Adhesive thickness: 0.03 mm (1.2 mil)

c) Electrode insulation materials:
Covered electrode: 3M Scotch-Seal No. 229 pads
Exposed electrode:
Kapton® (E.I. du Pont de Nemours and Company) 3M No. 5413, 0.08 mm (3 mil) thick (2 layers used)
Super Corona Dope®: MG Chemicals Inc. Cat. No. 4226-1L (3 to 4 layers used)

[**] http://www.azom.com as of May 24, 2016.

Acknowledgments

This project was supported by the National Aeronautics and Space Administration (NASA), Transformational Tools and Technologies (TTT) Project (formerly Aerospace Sciences Project), of the Aeronautics Research Mission Directorate.

References

[1] Moreau, E., "Airflow Control by Non-Thermal Plasma actuators," Journal of Physics. D: Applied Physics, Vol. 40, 2007, pp. 605–636.

[2] Corke, T. C., Post, M. L., and Orlov, D. M., "SDBD Plasma Enhanced Aerodynamics: Concepts, Optimization and Applications," Progress in Aerospace Sciences Vol. 43, 2007, pp. 193–217.

[3] Corke, T. C., Post, M. L., and Orlov, D. M., "Single Dielectric Barrier Discharge Plasma Enhanced Aerodynamics: Physics, Modeling and Applications," Experiments in Fluids, Vol. 46, 2009, pp. 1–26.

[4] Corke, T. C., Enloe, C. L., and Wilkinson, S. P., "Dielectric Barrier Discharge Plasma Actuators for Flow Control," Annual Reviews of Fluid Mechanics, Vol. 42, 2010, pp. 505–29.

[5] Roupassov, D. V., Nikipelov, A. A, Nudnova, M. M., and Starikovskii, A. Yu., "Flow Separation Control by Plasma Actuator with Nanosecond Pulse Periodic Discharge," AIAA Paper 2008-1367, 2008

[6] Benard, N. and Moreau, E., "Electrical and Mechanical Characteristics of Surface AC Dielectric Barrier Discharge Plasma Actuators Applied to Airflow Control," Experiments in Fluids, Vol. 55, 2014, pg. 20141846 (43 pp).

[7] Kotsonis, M., "Diagnostics for Characterisation of Plasma Actuators," Measurement Science and Technology. Vol. 26, 2015, pg. 092001 (30pp).

[8] Starikovskiy, A., Gordon, S., Post, M., and Miles, R. "Barrier Discharge Development and Thrust Generation at Low and High Pressure Conditions," AIAA paper 2014-0329, January 2014.

[9] Ashpis, D.E., Laun M.C., "Thrust Measurement of Dielectric Barrier Discharge (DBD) Plasma Actuators," Bulletin of the American Physical Society , Series II, Vol. 58, No. 18 , November 2013, Paper No. M25.03, pp. 416-417.

[10] Ashpis, D.E., Laun M.C., "Dielectric Barrier Discharge (DBD) Plasma Actuators Thrust – Measurement Methodology Incorporating New Anti-Thrust Hypothesis," AIAA Paper 2014-0486, January 2014.

[11] Ashpis, D.E., Laun M.C., "Dielectric Barrier Discharge (DBD) Plasma Actuators: New Anti-Thrust Hypothesis, Frequency Sweeps Methodology, Humidity and Enclosure Effects," NASA/TM—2014-218115, July 2014.

[12] Glezer, A., and Amitay, M., "Synthetic Jets," Annual Reviews of Fluid Mechanics, Vol. 34, 2002, pp.:503–29.

[13] Hoskinson, A.R., Hershkowitz, N., and Ashpis, D.E., "Force Measurements of Single and Double Barrier DBD Plasma Actuators in Quiescent Air," Journal of Physics D: Applied Physics, Vol. 41, 2008, 245209 (9pp).

[14] Baughn, J.W., Porter, C.O., Peterson, B.L., McLaughlin, T.E., Enloe, C.L., Font, G.I., and Baird, C., "Momentum Transfer for an Aerodynamic Plasma Actuator with an Imposed Boundary Layer," AIAA paper 2006-168, 2006.

[15] Benard, N., Balcon, N., and E. Moreau, E., "Electric Wind Produced by a Surface Dielectric Barrier Discharge Operating Over a Wide Range of Relative Humidity," AIAA Paper 2009-488, 2009.

[16] Wilkinson, S., Siochi, E., Sauti, G., Xu, T-B., Meador, M.A., and Guo, H. "Evaluation of Dielectric-Barrier-Discharge Actuator Substrate Materials," AIAA paper 2014-2810, June 2014.

[17] Thomas, F.O., Corke, T.C., Iqbal, M., Kozlov, A., and Schatzman, D. "Optimization of Dielectric Barrier Discharge Plasma Actuators for Active Aerodynamic Flow Control," AIAA Journal, Vol. 47, No. 9, September 2009, pp 2169-2178.

[18] Zito, J.C., Arnold, D.P., Houba, T., Soni, J., Durcher, R.J., and Roy, S., "Microscale Dielectric Barrier Discharge Plasma Actuators: Performance Characterization and Numerical Comparison," AIAA Paper 2012-3091, 2012